Impedance measurements of *ex vivo* rat lung at different volumes of inflation

Michael L. Oelze,[a] Rita J. Miller, and James P. Blue, Jr.
Bioacoustics Research Laboratory, Department of Electrical and Computer Engineering, University of Illinois, 405 North Mathews, Urbana, Illinois 61801

James F. Zachary
Bioengineering Program, University of Illinois, 1406 West Green Street, Urbana, Illinois 61801

William D. O'Brien, Jr.
Bioacoustics Research Laboratory, Department of Electrical and Computer Engineering, University of Illinois, 405 North Mathews, Urbana, Illinois 61801 and Bioengineering Program, University of Illinois, 1406 West Green Street, Urbana, Illinois 61801

(Received 7 February 2003; revised 5 September 2003; accepted 15 September 2003)

A previous study [J. Acoust. Soc. Am. **111**, 1102–1109 (2002)] showed that the occurrence of ultrasonically induced lung hemorrhage in rats was directly correlated to the level of lung inflation. In that study, it was hypothesized that the lung could be modeled as two components consisting of air and parenchyma (contiguous tissue [pleura and septa]). The speed of sound and lung impedance would then depend on the fractional volume of air in the lung. According to that model, an inflated lung should act like a pressure-release surface for sound incident from tissue onto a tissue-lung boundary. A deflated lung containing less air should allow more acoustic energy into the lung tissue because the impedance was more closely matched to the contiguous tissues. In the study reported herein, a measurement technique was devised to calculate the impedance of seven rat lungs, *ex vivo*, under deflation (atmospheric pressure) and three volumes of inflation pressure (7-cm H_2O, 10-cm H_2O, and 15-cm H_2O). Lungs were dissected from rats and immediately scanned in a tank of degassed 37 °C water. The frequency-dependent acoustic pressure reflection coefficient was measured over a frequency range of 3.5 to 10 MHz. From the reflection coefficient, the frequency-dependent lung impedance was calculated with values ranging from an average of 1 Mrayls in deflated lungs to 0.2 Mrayls for fully inflated lungs. Lung impedance calculations showed that deflated lungs had an impedance closer to water (1.52 Mrayls) than inflated lungs. At all volumes of inflation, the lungs acted as pressure-release surfaces relative to the water. The average of the four lung impedance values (deflated, 7-cm H_2O, 10-cm H_2O, and 15-cm H_2O) at each level of inflation was statistically different ($p<0.0001$). © *2003 Acoustical Society of America.* [DOI: 10.1121/1.1624069]

PACS numbers: 43.80.Cs, 43.80.Gx, 43.80.Jz [FD] Pages: 3384–3393

I. INTRODUCTION

Studies have shown that ultrasound causes lung hemorrhage in animals.[1–17] The mechanism is unknown and under considerable debate; however, the interaction of ultrasound with gas bodies is the primary hypothesis.[18–23] Gas bodies include ''theoretical'' microbubbles within the surfactant layer of each alveolus (≈ 5 μm in diameter) and air in the alveolar architecture of the lung (≈ 40 μm in diameter for each murine alveolus).[24–26]

In vivo experiments in rats demonstrated that deflated lung (lower gas volume) increased the occurrence and degree of hemorrhage when compared to a fully inflated lung.[27] This study hypothesized that the amount of ultrasonic energy transmitted into the lung was inversely related to the volume of inflation. The lung was modeled as bulk material consisting of tissue and air. The less air in the lung, the more the impedance of the lung matched the impedance of adjacent intercostal tissues. The more air in the lung, the greater was the mismatch in impedance between the lung and the surrounding tissues. When the impedance of the lung more closely matched the impedance of the intervening tissues, more ultrasonic energy was transmitted into the lung itself. Thus, a higher occurrence and severity of lung damage resulted in a deflated lung as opposed to an inflated lung.

Previous experiments supported the bulk model of the lung.[28] In these experiments, canine lungs of varying volumes of inflation were fixed and then sliced for measurement of the attenuation and reflection loss. The results showed that the reflection losses were less for inflated lungs than for deflated lungs. Furthermore, the experiments on the canine lungs showed the reflection loss had a frequency dependence.

Several other studies have looked at the propagation of ultrasound in the lung. Dunn and Fry studied the attenuation of ultrasound in freshly excised lungs of dogs at frequencies of 1, 2.25, and 5 MHz and showed that the attenuation had a logarithmic dependence.[29,30] Measurements of sound speed in the lungs showed that the speed of sound was slightly

[a]Electronic mail: oelze@brl.uiuc.edu

linear with frequency.[31] Further studies on lungs with different volumes of inflation yielded increasing attenuation and decreasing sound speed with increased inflation.[31] Studies by Pederson and Ozcan involving cow lungs over the frequency range of 10 to 800 kHz showed measured group velocities had a strong dependence on inflation level, and attenuation exhibited a strong frequency dependence that was weakly dependent on inflation level.[32] A more recent study of ultrasound in pig lungs showed attenuation was large even in deflated lungs.[33] Therefore, in summary, the cumulative interpretation of results from these studies suggest that the amount of ultrasonic energy transmitting into and propagating within a deflated lung is much greater than in an inflated lung.

In the study reported herein, a technique was developed to measure the reflection coefficient and calculate impedance value of intact, fresh lungs, *ex vivo*, from rats for different volumes of inflation. It was hypothesized that fresh lung would have an impedance value dependent on the frequency and volume of inflation. It was previously hypothesized that the impedance value of the lung due to inflation was related to the occurrence of lung damage in rats.[27] Section II describes the theory of lung impedance and its relation to the pressure reflection coefficient. Section III details a new procedure to measure impedance values from fresh, whole lungs. Section IV presents the results of the measurements and the final section (V) gives some conclusions about the study.

II. THEORY

The acoustic pressure reflection coefficient (for plane waves) for sound reflecting at normal incidence from a smooth boundary of two different media (medium I, II) is defined as[34]

$$R=\frac{P_R}{P_I}, \tag{1}$$

where P_R is the amplitude of the reflected sound, and P_I is the amplitude of the incident pressure wave. The sign of R was theorized to be negative because the impedance of the lung (medium II composed of tissue and air) was presumed less than water (medium I). Subsequent measurements from the lung verified that the lung acted as a pressure relief surface relative to water. The pressure reflection coefficient can be measured by comparing the signal reflected, P_R, from the surface of medium II with the sound incident, P_I, on the surface. If a transducer is operated in pulse-echo mode to measure the pressure pulse reflected from the surface, then the pressure amplitude of the reflected signal is found by

$$P_R=S_{\mathrm{Re}}V_R, \tag{2}$$

where V_R is the voltage signal recorded from the received signal and S_{Re} is the receive sensitivity of the pulse-echo transducer.

The incident pressure and the sensitivity of the transducer to receive can be factored out in the measurement of the reflection coefficient by using a reference pulse. The reference pulse is found by using the same settings, equipment, and transducer to reflect a signal from a planar surface of known reflectivity, R_{ref}. Dividing the unknown reflection coefficient, R, by the known reflection coefficient yields

$$\frac{R}{R_{\mathrm{ref}}}=\frac{S_{\mathrm{Re}}V_R/P_I}{S_{\mathrm{Re}}V_{\mathrm{ref}}/P_I}, \quad \frac{R}{R_{\mathrm{ref}}}=\frac{V_R}{V_{\mathrm{ref}}}. \tag{3}$$

Solving for R gives

$$R=\frac{V_R}{V_{\mathrm{ref}}}R_{\mathrm{ref}}, \tag{4}$$

where V_{ref} is the voltage measured from the signal reflected from the surface of the known reflector.

For many surfaces, the reflection coefficient is not constant with frequency. The frequency dependence of the reflection coefficient can be found by taking the magnitude of the Fourier transform of the voltage signals, V_R and V_{ref}. Assuming that the reflection coefficient from the plastic plate is constant with frequency, then

$$|R(f)|=\frac{|FT\{V_R(t)\}|}{|FT\{V_{\mathrm{ref}}(t)\}|}R_{\mathrm{ref}}. \tag{5}$$

The reflection coefficient will be positive or negative depending on the impedance change from one medium to another. If the second medium has a smaller impedance value than the first medium (a pressure release surface), then the pressure reflection coefficient will be negative. If the second medium has larger impedance than the first medium, then the pressure reflection coefficient will be positive.

The pressure reflection coefficient is related to the impedance of the two media by[34]

$$R(f)=\frac{Z_{II}(f)-Z_I(f)}{Z_{II}(f)+Z_I(f)}, \tag{6}$$

where $Z_I(f)$ and $Z_{II}(f)$ represent the impedance of media I and II, respectively. Solving Eq. (6) for the impedance of medium II yields

$$Z_{II}(f)=Z_I(f)\frac{1+R(f)}{1-R(f)}. \tag{7}$$

If the impedance of medium I is known (i.e., water) and the pressure reflection coefficient at the boundary of media I and II is measured, the impedance of medium II can be determined through Eq. (7).

In our previous study, the lung was modeled as two components consisting of air and tissue.[27] The lung's density was modeled as a composite of the fractional volume of air, x_{air}, in the lung and the fractional volume of tissue, $x_{\mathrm{parenchyma}}$, giving

$$\rho_{\mathrm{lung}}=x_{\mathrm{air}}\rho_{\mathrm{air}}+x_{\mathrm{parenchyma}}\rho_{\mathrm{parenchyma}}, \tag{8}$$

where $x_{\mathrm{air}}+x_{\mathrm{parenchyma}}=1$. The adiabatic bulk modulus of the lung was also modeled as a composite of air and tissue

$$B_{\mathrm{lung}}=x_{\mathrm{air}}B_{\mathrm{air}}+x_{\mathrm{parenchyma}}^{3.5}B_{\mathrm{parenchyma}}. \tag{9}$$

The propagation speed and acoustic impedance could then be determined according to

$$c_{\mathrm{lung}}=\sqrt{B_{\mathrm{lung}}/\rho_{\mathrm{lung}}} \tag{10}$$

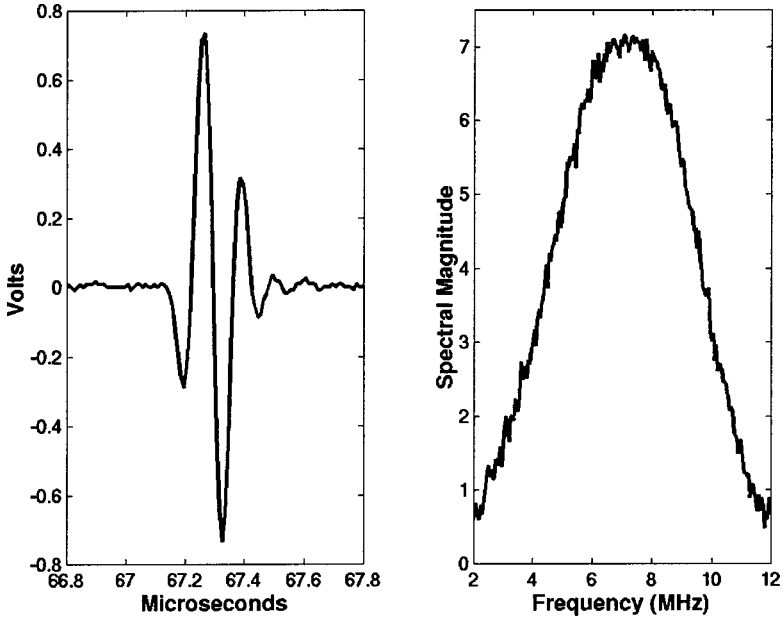

FIG. 1. Acoustic pulse (left) reflected from the plastic plate and the magnitude of the Fourier spectrum (right) of the pulse reflected from the plastic plate.

and

$$z_{\text{lung}} = \sqrt{\rho_{\text{lung}} B_{\text{lung}}}. \tag{11}$$

Previously published values for measurements of the density and bulk properties of air and lung yielded $\rho_{\text{air}} = 1.21\ \text{kg/m}^3$, $\rho_{\text{parenchyma}} = 600\ \text{kg/m}^3$, $B_{\text{air}} = 142\ \text{kPa}$, and $B_{\text{parenchyma}} = 1\ \text{GPa}$.[27] If the volume fraction of air is large (i.e., fully inflated lung), then the lung's adiabatic bulk modulus and the lung's density both will be closer to the values for air. The impedance of the fully inflated lung will be closer to the impedance of air and will act as a pressure release boundary relative to water. On the other hand, a lung with a small amount of air (deflated lung) will have an impedance closer to water or tissue. According to the model, less ultrasonic energy will be transmitted into an inflated lung than into a deflated lung because the impedance of a deflated lung is more closely matched to the impedance of tissue or water. The model has been used to explain the greater percentage of lesion occurrence in the deflated lungs of rats as opposed to inflated lungs.[27]

III. MEASUREMENT METHODS

A. Ultrasound measurement device

A single-element weakly focused ultrasonic transducer (GE Panametrics Inc., Waltham, MA) was used to make measurements of the reflection coefficient from planar reflectors and the lung tissues. The transducer had an aperture diameter of 19 mm and a focal length of 51 mm measured from a planar reflector. The center frequency of the transducer was 7.1 MHz with a −6-dB pulse-echo frequency bandwidth of 5.5 MHz and a −6-dB pulse-echo beamwidth of ~550 μm. The analysis bandwidth ranged from 3.5 to 10 MHz (−9-dB pulse-echo bandwidth). Figure 1 shows the reflected pulse from a flat plastic plate at the focus of the transducer and the corresponding Fourier spectrum (magnitude) of the reflected pulse. The transducer was operated in pulse-echo mode through a Panametrics 5800 pulser/receiver (GE Panametrics, Inc., Waltham, MA). The amplitude of the pulse used for the reflection coefficient study was 1.4 MPa. The signals were recorded with a calibrated PVDF membrane hydrophone (Marconi Model Y-34-6543, Chelmsford, UK) and digitized on an oscilloscope (LeCroy 9354TM, Chestnut Ridge, NY) that had a dynamic range of 48 dB and downloaded to a PC computer for post-processing. The sampling rate was 50 MHz. Reflection measurements were taken near the focus of the transducer where the sound field could be approximated as plane waves.

While the planar reflector is a flat surface, the lung is not a flat surface. One of the difficulties in the experimental setup was to align the lung with the transducer so that the sound reflected from the lung was at normal incidence. Failure to align the lung properly or local curvature of the lung surface would lead to a reduced reflected signal relative to sound reflected at normal incidence. To quantify the possible alignment error, the plastic plate was used to record the relative reflected signal at several angles of incidence. A smooth plastic plate was placed normally incident to the transducer at the focus and rotated axially several degrees. Figure 2 shows a diagram of the plastic plate and transducer setup. The plastic plate was rotated about the z-axis and the magnitude of the signal decrease was then recorded. Figure 3 shows the relative pulse intensity integral (PII) of the reflected signal as the angle of incidence changes from normal. The angle of incidence could be off normal by 2.5° and still have a PII value within 10% error of true normal.

The lung surface was measured similarly to the reflection from the plastic plate. In order to obtain a smooth, flat surface on the lung that would be near normal incidence, the lung was gently pressed up against a plastic holder that was aligned perpendicular to the beam axis. The holder had a small circle cut out in the middle with a diameter of 18 mm that allowed for a scanning window onto the lung surface; the lung surface was in direct contact with the water. The large size of the scanning window (18 mm) compared to the beamwidth (~550 μm) ensured negligible diffraction effects.

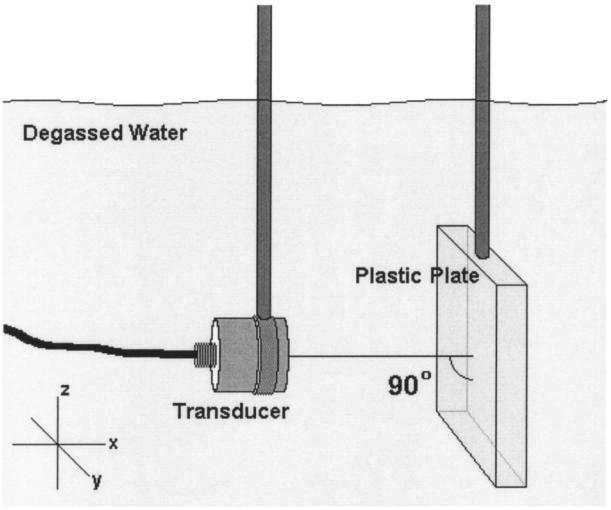

FIG. 2. Experimental setup of the transducer reflecting a pulse at normal incidence from a plastic plate of known reflectivity through a water path.

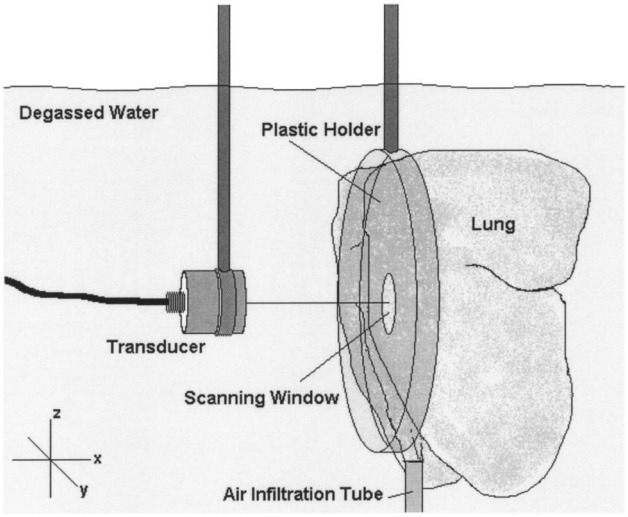

FIG. 4. Experimental setup of the transducer reflecting a pulse from a lung surface through a water path.

Figure 4 shows a diagram of the lung and transducer setup. The lung was set up so that its surface would be near the focus of the transducer. A 5 mm×5 mm square perpendicular to the beam axis of the transducer (*y*, *z* plane) was scanned on the surface of the lung. The rf data waveforms were acquired at intervals of 100 μm in the *y* and *z* directions. Figure 5 shows a pulse reflected from the surface of a lung along with the accompanying Fourier spectrum (magnitude) of the reflected pulse. Scanned results were downloaded to a computer for postprocessing.

Reference pulses were measured from a smooth plastic plate of known reflectivity and a smooth air–water interface. The transducer was aligned perpendicular to the reflecting surface. The same equipment and settings were used for the pulse/echo measurement of the reference pulse as used for the lung reflection measurements. Reflection measurements from the planar surfaces were made at different depths relative to the transducer by scanning axially along the transducer beam. The scan measured reflected values over an axial length of 1 cm centered about the focus with a step size of 100 μm (approximately half the wavelength).

To test the validity of the approach, measurements were taken from a water–air interface and a water–Dow Corning 710 interface. The speed of Dow Corning 710 (1340 m/s) is published and the density (1.11×10^3 kg/m^3) can be found from Dow Corning Corporation (Midland, MI).[35] The water–Dow Corning 710 interface measurements were taken in a water bath temperature of 22.2 °C, making the impedance of the water larger than the impedance of the Dow Corning 710 oil. Figure 6 shows the percent error in the measured impedance of the Dow Corning 710 oil from the published values using the measurement technique described in this study. Figure 7 shows the percent error between the measured and theoretical pressure reflection coefficients for the water–air interface. The small difference between the theoretical and measured values show the measurement technique is valid.

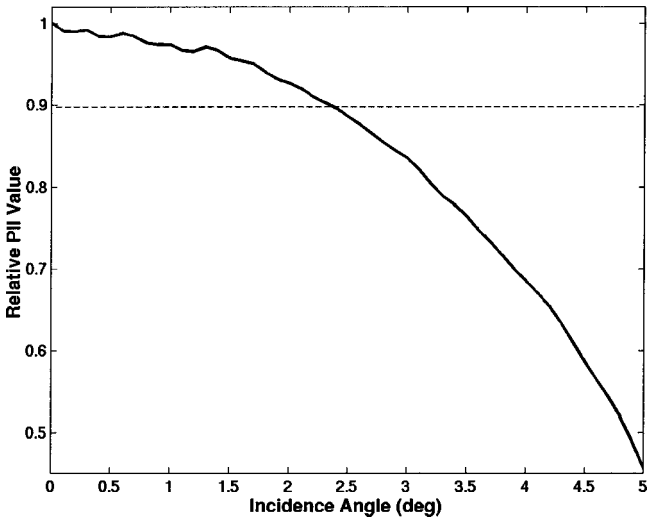

FIG. 3. Relative loss in magnitude of the PII value of reflected signal as the angle of incidence moves away from normal.

B. Animal procedures

The experimental protocol was approved by the Laboratory Animal Care Advisory Committee at the University of Illinois at Urbana—Champaign and satisfied all campus and NIH (National Institutes of Health) rules for the humane use of laboratory animals. Rats were housed in an Association for Assessment and Accreditation of Laboratory Animal Care, Rockville, MD (AAALAC)-approved animal facility, placed in groups of 1–3 in polycarbonate cages with beta-chip bedding and wire bar lids, and provided food and water *ad libitum*. The AAALAC is a private, nonprofit organization that promotes the humane treatment of animals in science through a voluntary accreditation program.

Seven 16-to-20-week-old (240-to-280-g) female Sprague-Dawley rats (Harlan, Indianapolis, IN) were weighed and anesthetized with ketamine hydrochloride (87.0 mg/kg) and xylazine (13.0 mg/kg) administered intraperitoneally. Rats were immediately euthanized while under anesthesia by cervical dislocation. The lungs (with heart still at-

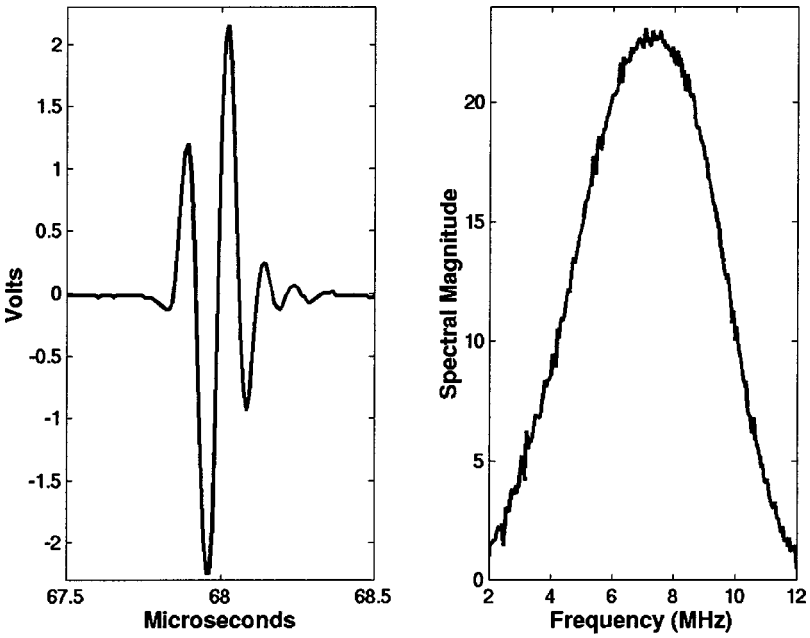

FIG. 5. Acoustic pulse (left) reflected from an inflated lung surface and the magnitude of the Fourier spectrum (right) of the pulse reflected from the lung surface.

tached) and trachea were removed by opening the thorax with a midline incision. Following removal, the lungs were rinsed with 0.9% saline solution. Saline was not allowed to enter the trachea. All lungs were used immediately post harvest.

A 20-gauge needle, with the tip blunted, was inserted into the trachea, which was sealed airtight around the needle hub. Plastic hosing was then used to attach the needle to the lung inflation apparatus. The lung inflation apparatus consisted of a plastic tube connected to two pressure regulators, a tank of compressed air, and a ruler to determine the pressure level (Fig. 8). Pressure in the lungs was measured in terms of cm of H_2O ($1\ \text{cm}\ H_2O = 98\ \text{Pa}$). When a pressure level of 30-cm H_2O in the *ex vivo* lungs was reached, the lung was considered fully inflated or inflated to total lung capacity.[36]

All measurements were taken in degassed water at $37 \pm 0.5\ ^\circ\text{C}$. Water temperature was controlled by a proportional temperature controller (Yellow Springs Instrument Co., Inc., Yellow Springs, OH). A digital thermometer (Control Company, Friendswood, TX), with an accuracy of $0.2\ ^\circ\text{C}$, in the water tank served as the temperature standard. During the time frame of the experimental procedures, the lung did not undergo significant degradation in the degassed water because the visceral pleura of the lung consists of structural proteins (i.e., fibers).

Measurements of the ultrasound reflection coefficient were taken at four different volumes of inflation for each rat lung. The first measurements of the ultrasound reflection coefficient were taken on the deflated lungs (0-cm H_2O). After the deflated measurement was taken, the lung was slowly inflated, at a rate of 1-cm H_2O per minute, to 20-cm H_2O. The lung was held at that pressure for a minimum of 5 min to allow the pressure and air inside the lung to equilibrate. The pressure was then reduced to 15-cm H_2O, at 2-cm H_2O per minute, and held for 15 min to ensure pressure equilibrium. Measurements of the ultrasound reflection coefficient were taken from the inflated lung at 15-cm H_2O. For a normal

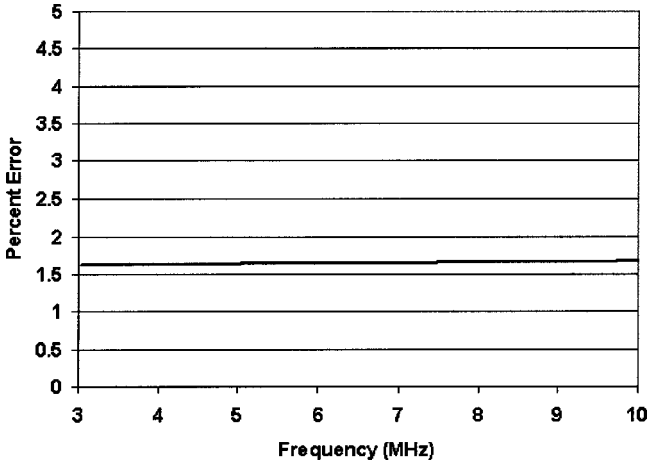

FIG. 6. Plot of the percent difference between the measured and theoretical impedance values versus frequency using the reference spectrum technique for Dow Corning 710.

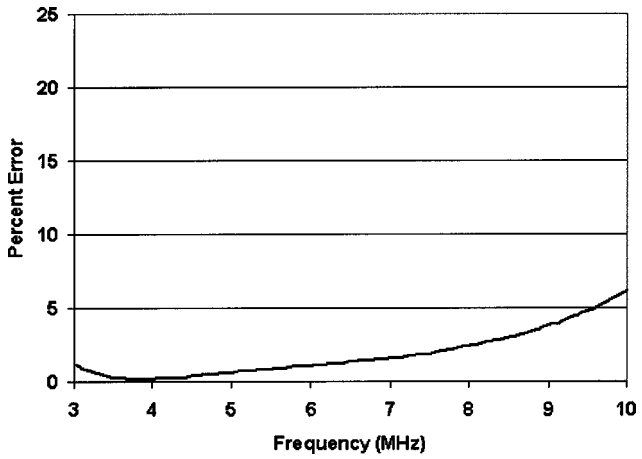

FIG. 7. Plot of the percent difference between the measured and theoretical pressure reflection coefficient using the reference spectrum technique for the water/air interface.

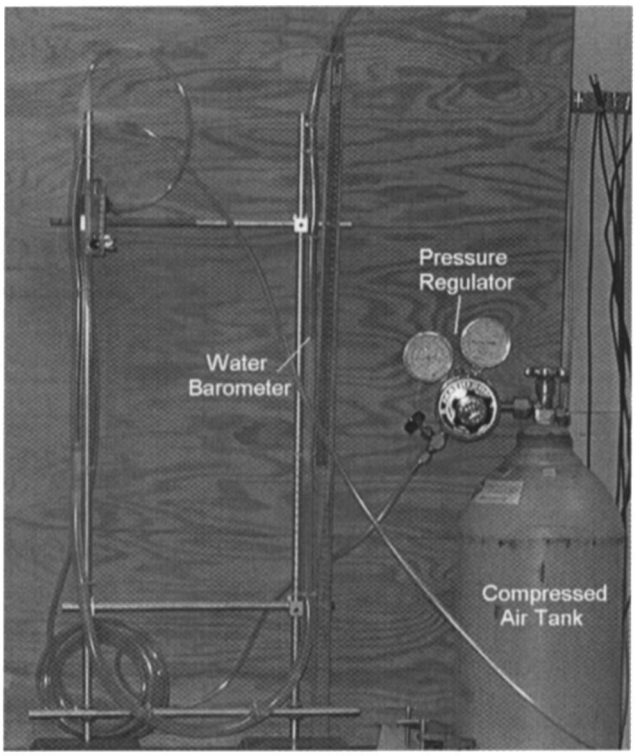

FIG. 8. Picture of the inflation apparatus including compressed air tank, pressure gauge regulators and water barometer.

animal, 15- to 20-cm H_2O pressure is required for adequate but not full inflation.[37] The next two pressure volumes were used to observe lung impedance as the pressure level was reduced below the level necessary to inflate the lung. The pressure was reduced to 10-cm H_2O and 7-cm H_2O, at 2-cm H_2O per minute, and held for 15 min at each pressure level to ensure pressure equilibrium. Measurements of the ultrasound reflection coefficient were taken from the inflated lung at 10-cm and 7-cm H_2O. The 7-cm H_2O was the lowest pressure that could be maintained without the lung visibly deflating during the measurement procedure.

C. Data analysis

Waveforms acquired by the transducer were downloaded to a computer for postprocessing. Matlab® (The Mathworks Inc, Natick, MA) was used to perform the waveform analysis. In order to reduce measurement error of reflections from off-normal incidence, waveform sections were used in the calculations that coincided with flat areas at near-normal incidence on the lung surface. A surface plot of the lung over the 5×5 mm^2 scanned area was constructed from the waveforms. The surface plot was constructed by finding the distance from the source to the peak with the maximum magnitude in each reflected waveform. Figure 9 shows a graph of a surface plot from one of the rat lungs. The flat regions shown by the surface plots were used to determine smooth regions at near-normal incidence from which the reflection coefficient calculations were made. The angle of incidence at a particular point in the scan region was calculated from the average of the arctangents of the slopes between the particular scan point and four immediately surrounding scan points. Only reflected pulses from scan points that showed angles of incidence less than 0.5° from normal were used.

The frequency dependence of each waveform in the selected region was calculated by taking the Fourier transform. Each reflection waveform was made up of 2000 points. A Hanning window was constructed based on the width of the pulse reflected from the reference surface. The Hanning window was applied to the pulse reflected from the lung by centering the window at the point in the waveform where the peak had its maximum magnitude. The size of the deflated rat lung was more than a centimeter in diameter while the length of the pulse was around 300 μm, enabling the gating out of multiple surface echoes. The Hanning window was also applied in the same manner to the pulse reflected from the planar (reference) surface. The absolute values of the Fourier transforms from the waveforms were taken and all the Fourier spectra were averaged together from the selected region to obtain an overall representation of the reflection from the region specified. The average of the Fourier spectra

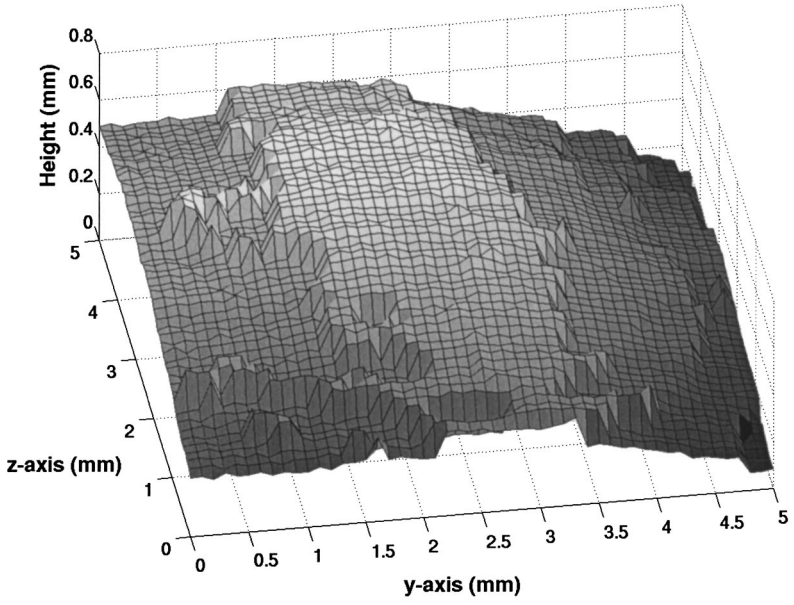

FIG. 9. Surface plot of the lung recorded from the maximum peak magnitude of waveforms scanned over a 5×5 mm^2 window.

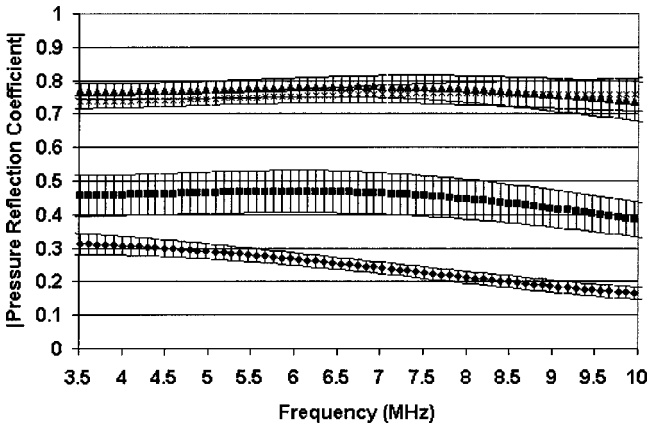

FIG. 10. Plot of the average magnitude of the pressure reflection coefficient from 7 rats versus frequency for four inflation volumes, ♦, pressure of 0.0-cm H_2O (deflated case); ■, pressure of 7-cm H_2O; ▲, pressure of 10-cm H_2O; ×, pressure of 15-cm H_2O. Error bars represent $\frac{1}{2}$ standard deviation about the mean for seven rats.

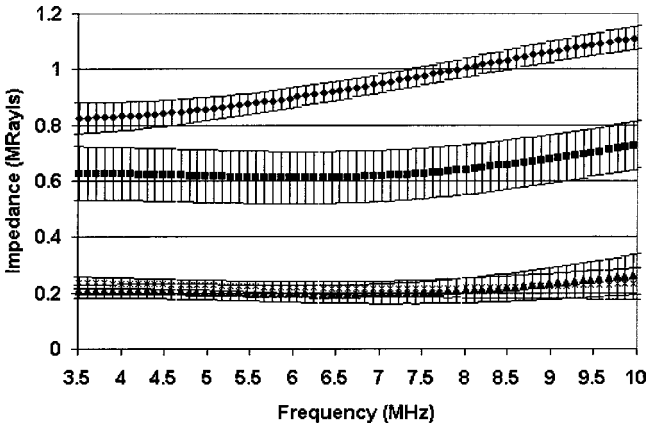

FIG. 11. Plot of the average impedance value from seven rats versus frequency for four inflation volumes, ♦, pressure of 0.0-cm H_2O (deflated case); ■, pressure of 7-cm H_2O; ▲, pressure of 10-cm H_2O; ×, pressure of 15-cm H_2O. Error bars represent $\frac{1}{2}$ standard deviation about the mean for seven rats.

was then divided by the reference spectrum and multiplied by the appropriate reflection coefficient for the reference surface according to Eq. (5).

The impedance was then calculated over the frequency range of 3.5–10 MHz according to Eq. (7) where $Z_I(f)$ represented the characteristic acoustic impedance of water at 37 °C, $Z_I(f)=\rho_{H_2O}c=1.52$ MRayls (ρ_{H_2O} is the density of water, 998 kg m^{-3}, and c is the speed of sound in water at 37 °C, 1525 m s^{-1}). The sign of the reflection coefficient was determined by comparing the reflected pulses from the plastic plate and the lung surface. A comparison of the reflected pulses from Figs. 1 and 5 shows that the pulse reflected from the lung surface was 180° out of phase with the pulse reflected from the plastic plate. Because the plastic plate's impedance was greater than the surrounding water, the opposite sign from the pulse reflected from the lung meant the lung surface represented a pressure relief type of surface. The sign change of the reflected pulse from the plastic plate to the lung was evident at all inflation volumes. In calculating the impedance of the lung surface from Eq. (7), a minus sign was multiplied times the magnitude of the reflection coefficient yielding impedance estimates according to

$$Z_{II}(f)=\rho_{H_2O}c\,\frac{1-|R(f)|}{1+|R(f)|}. \tag{12}$$

IV. RESULTS

The procedure was applied to the four different inflation volumes and graphed for comparison. Figure 10 shows the graph of the average measured reflection coefficient magnitudes versus frequency for the four different inflation volumes. Each data point represents the average of measurements taken from seven different rat lungs. The smallest reflections came from the deflated cases and the largest overall reflections came from the most inflated cases.

Figure 11 shows the average impedance values versus frequency calculated for the seven rat lungs at different inflation volumes. The data show that the more deflated the lung, the closer the impedance value was to water (1.52 MRayls). The closer the impedance of the lung was to water, the more energy was transmitted into the lung itself. Likewise, for the most inflated level of the lung, the impedance had the greatest disparity from water meaning that relatively less energy was being transmitted into the lung. Volumes of inflation between fully inflated and deflated appeared to have impedance values between the deflated and fully inflated cases.

The linear regression analysis was performed on the impedance values for each of the four volumes of inflation (Fig. 12).[38] The linear regression analysis yielded the p-value for the slope, the ±95% confidence band for the regression line and the coefficient of determination, r^2. As a function of frequency (range: 2.15–12.0 MHz), the linear regression equations for each the four volumes of inflation from the seven rat lungs were

$$Z_{\text{deflated}}=0.040f+0.68\ \ (n=714;p<0.0001;r^2=0.34), \tag{13a}$$

$$Z_{7\text{-cm}}=0.019f+0.53\ \ (n=714;p<0.0001;r^2=0.026), \tag{13b}$$

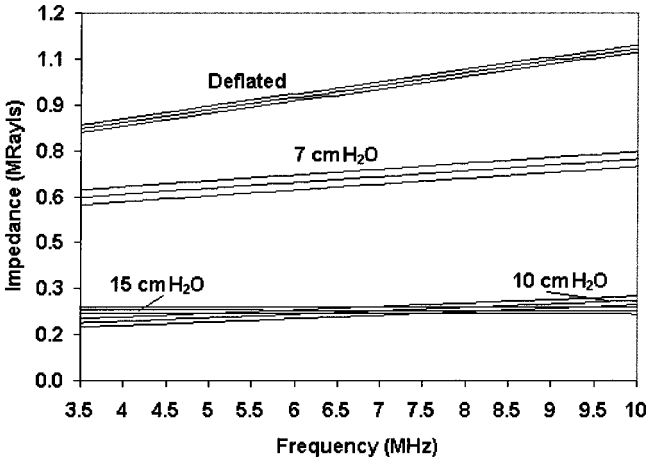

FIG. 12. Linear fits to the impedance data with 95% confidence intervals.

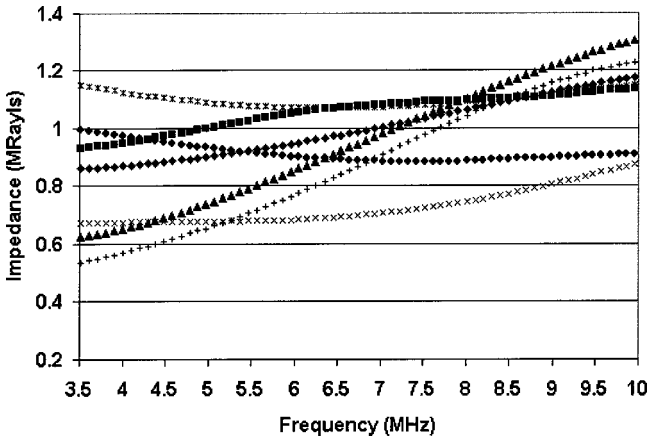

FIG. 13. Impedance values for the seven rats measured from deflated lungs.

$$Z_{10\text{-cm}} = 0.011f + 0.15 \quad (n = 714; p < 0.0001; r^2 = 0.027), \tag{13c}$$

$$Z_{15\text{-cm}} = -0.00027f + 0.23 \quad (n = 714; p = 0.89; r^2 < 0.001), \tag{13d}$$

where the acoustic impedance, Z, is in MRayl and the ultrasonic frequency, f, is in MHz.

To test for equality of the four regression lines for each of the four volumes of inflation an analysis of covariance F-test was performed.[38] The null model constrains the intercepts and slopes to be equal across different volumes of inflation. The general model allows for unequal intercepts and slopes for the volumes of inflation. If not rejected, then the null model is used. If it is rejected, then the general model is used. Comparison of the acoustic impedances in the general model for the four volumes of inflation indicates that the four linear regressions are different ($p < 0.0001$). Likewise, comparison of the acoustic impedances in the general model for the two most inflated cases (10-cm H_2O and 15-cm H_2O) indicates that the two linear regressions are different ($p < 0.0001$).

The previous graphs of the impedance (Figs. 11 and 12) showed general trends for the lungs from the seven rats. The deflated lungs tended to transmit more ultrasound energy into the lung than the inflated lungs. In a case by case examination, each lung will be different with different ultrasonic properties. Figure 13 shows the frequency-dependent impedance values for the seven rat lungs under deflation. The graph shows a definite spread of the measured impedance values from one rat to another. In the previous study, the deflated lungs had the greatest occurrence of ultrasound-induced lesions, though not all of the rat lungs developed lesions.[27] Figure 13 may help explain the fact that under the same exposure conditions some rats will develop lesions while others do not. In general, the deflated lungs will admit more acoustic energy than inflated lungs, but individual lungs will vary in the magnitude of ultrasonic energy transmitted into the lung under deflation. A similar spread in the data was also seen for the inflated lungs showing the biological variability from one animal to the next.

The frequency dependence for the two most inflated cases (10-cm H_2O and 15-cm H_2O) appeared to be minimal but increased as the level of inflation decreased. The cause of the frequency dependence may be due to increasing roughness of the lung surface with deflation. When the lung was inflated, the visceral pleura was stretched taught and appeared to be smooth. In a deflated lung, the loose visceral pleura may have bunched together causing the surface to be less smooth. The morphologic structure of the surface of the lung (visceral pleura) is very uniform in all species but varies in thickness and fiber composition (i.e., density and type) between species. In the inflated state, the visceral pleura of the lung is stretched very taught such that the topographical features of the surface are smooth no matter where the lung is acoustically examined. In the deflated state, the visceral pleura is no longer stretched and is likely contracted such that the topographical features of the surface are ''roughened'' or irregular from area to area examined acoustically. If the roughness is small relative to the wavelength of sound, most of the acoustic energy will be reflected back to the source. As the wavelength becomes smaller relative to the roughness, more acoustic energy is scattered or reflected off in different directions, reducing the amount of acoustic energy reflected back to the source. Figure 10 shows that the higher frequencies (smaller wavelengths) reflected back less sound than the lower frequencies (larger wavelengths). In the case of the deflated lung, the impedance measurement of the lung surface may be a combination of the true lung impedance and surface roughness properties of the lung.

The frequency dependence of the reflection coefficient from the deflated lung may also be due to the amount of energy transmitted into the deflated lung. With the inflated lungs, a single pulse is seen reflected from the lung surface because almost no acoustic energy is transmitted into the lung. In the case of the deflated lung, the return echo tends to have a train of pulses returning (speckle). The train of pulses in the echo suggests that sound is returning from inside the lung as well as from the surface of the lung. It is possible that the pulses corresponding from within the lung are interfering with the sound reflecting from the surface. The interference of the pulses can cause apparent frequency dependence in the windowed waveform used to calculate the reflection coefficient. However, the effects of interference are minimal because on average the backscatter pulses trailing the surface reflection are more than 13 dB less than the surface reflection.

Comparison of the results obtained with the technique used in this study with the results from previous techniques and studies show similar trends. At frequencies of 5.0 and 7.4 MHz, Bauld and Schwan showed a decrease in the reflection coefficient from the inflated to deflated lung of 13 and 25 dB, respectively.[28] Results from Fig. 10 show a decrease from the inflated case to the deflated case of approximately 12 dB for the rat lungs for both 5.0 and 7.4 MHz. Both studies showed that the reflection loss increased with decreasing inflation. The frequency dependence observed by Bauld and Schwan was markedly greater than the frequency dependence observed in the present study.

V. CONCLUSIONS

Measurements were made at four volumes of inflation of the impedance of rat lungs. The measurements showed that the greater the volume of the inflation, the smaller the impedance value of the lung. Measurements also showed that the impedance value of the lung was always less than the characteristic impedance of water at 37 °C (pressure release surfaces relative to water). The fully inflated lungs were more similar to a water–air interface.

The impedance of the lungs at deflation was closer to the characteristic impedance value of water than for the inflated cases. More ultrasonic energy was transferred into the deflated lungs than into the inflated lungs. The same will also be true for ultrasonic incident on the lung from adjacent intercostal tissues. Most of the sound is reflected from the lung surface with just a little inflation. If increased ultrasonic energy transmitted into the lung causes an increase in the incidence of lung damage, then the increased ultrasonic energy transmitted into the deflated lung, due to a more closely matched impedance, supports earlier measurements of higher probability of lung lesions in rats with deflated lungs. However, further study needs to be conducted to show the exact cause of ultrasound induced lung damage.

For the inflated lungs, almost no frequency dependence was observed. Noticeable frequency dependence was seen for the deflated lung. The amount of ultrasonic energy reflected from the deflated lung appeared to decrease with higher frequencies of ultrasound. The more energy that was transmitted into the lung (deflated), the larger the frequency dependence was observed. Several factors may have contributed to the frequency dependence seen in the deflated lungs. Future experiments will examine whether the frequency dependence is due to lung impedance effects, surface roughness of the lung, interference of the surface reflection with pulses returning from within the lung or some other cause.

ACKNOWLEDGMENTS

The authors thank Steven Fay for his invaluable assistance in building the lung inflation apparatus. This work was supported by NIH Grant No. EB02641 (formerly HL58218) awarded to WDO and JFZ.

[1] S. Z. Child, C. L. Hartman, L. A. Schery, and E. L. Carstensen, "Lung damage from exposure to pulsed ultrasound," Ultrasound Med. Biol. **16**, 817–825 (1990).
[2] C. Hartman, S. Z. Child, R. Mayer, E. Schenk, and E. L. Carstensen, "Lung damage from exposure to fields of an electrohydraulic lithotriptor," Ultrasound Med. Biol. **16**, 675–679 (1990).
[3] D. P. Penney, E. A. Schenk, K. Maltby, C. Hartman-Raeman, S. Z. Child, and E. L. Carstensen, "Morphologic effects of pulsed ultrasound in the lung," Ultrasound Med. Biol. **19**, 127–135 (1993).
[4] C. H. Raeman, S. Z. Child, and E. L. Carstensen, "Timing of exposures in ultrasonic hemorrhage of murine lung," Ultrasound Med. Biol. **19**, 507–517 (1993).
[5] L. A. Frizzell, E. Chen, and C. Lee, "Effects of pulsed ultrasound on the mouse neonate: Hind limb paralysis and lung hemorrhage," Ultrasound Med. Biol. **20**, 53–63 (1994).
[6] J. F. Zachary and W. D. O'Brien, Jr., "Lung lesions induced by continuous- and pulsed-wave (diagnostic) ultrasound in mice, rabbits, and pigs," Vet. Pathol. **32**, 43–54 (1995).
[7] C. H. Raeman, S. Z. Child, D. Dalecki, C. Cox, and E. L. Carstensen, "Exposure-time dependence of the threshold for ultrasonically induced murine lung hemorrhage," Ultrasound Med. Biol. **22**, 139–141 (1996).
[8] W. D. O'Brien, Jr. and J. F. Zachary, "Lung damage assessment from exposure to pulsed-wave ultrasound in the rabbit, mouse, and pig," IEEE Trans. Ultrason. Ferroelectr. Freq. Control **44**, 473–485 (1997).
[9] D. Dalecki, S. Z. Child, C. H. Raeman, D. P. Penney, C. Cox, and E. L. Carstensen, "Age dependence of ultrasonically induced lung hemorrhage in mice," Ultrasound Med. Biol. **23**, 767–776 (1997).
[10] C. K. Holland, K. Sandstrom, X. Zheng, J. Rodriguey, and R. A. Roy, "The acoustic field of a pulsed Doppler diagnostic ultrasound system near a pressure release surface," J. Acoust. Soc. Am. **95**, 2855 (1994).
[11] W. D. O'Brien, Jr., L. A. Frizzell, D. J. Schaeffer, and J. F. Zachary, "Superthreshold behavior of ultrasound-induced lung hemorrhage in adult mice and rats: Role of pulse repetition frequency and exposure duration," Ultrasound Med. Biol. **27**, 267–277 (2001).
[12] J. F. Zachary, J. M. Sempsrott, L. A. Frizzell, D. G. Simpson, and W. D. O'Brien, Jr., "Superthreshold behavior and threshold estimation of ultrasound-induced lung hemorrhage in adult mice and rats," IEEE Trans. Ultrason. Ferroelectr. Freq. Control **48**, 581–592 (2001).
[13] J. F. Zachary, L. A. Frizzell, K. S. Norrell, J. P. Blue, Jr., R. J. Miller, and W. D. O'Brien, Jr., "Temporal and spatial evaluation of lesion reparative responses following superthreshold exposure of rat lung to pulsed ultrasound," Ultrasound Med. Biol. **27**, 829–839 (2001).
[14] W. D. O'Brien, Jr., D. G. Simpson, L. A. Frizzell, and J. F. Zachary, "Superthreshold behavior and threshold estimation of ultrasound-induced lung hemorrhage in adult rats: Role of beamwidth," IEEE Trans. Ultrason. Ferroelectr. Freq. Control **48**, 1695–1705 (2001).
[15] A. F. Tarantal and D. R. Canfield, "Ultrasound-induced lung hemorrhage in the monkey," Ultrasound Med. Biol. **20**, 65–72 (1994).
[16] R. Baggs, D. P. Penney, C. Cox, S. Z. Child, C. H. Raeman, D. Dalecki, and E. L. Carstensen, "Thresholds for ultrasonically induced lung hemorrhage in neonatal swine," Ultrasound Med. Biol. **22**, 119–128 (1996).
[17] D. Dalecki, S. Z. Child, C. H. Raeman, C. Cox, and E. L. Carstensen, "Ultrasonically induced lung hemorrhage in young swine," Ultrasound Med. Biol. **23**, 777–781 (1997).
[18] R. E. Apfel, "Comment on 'Ultrasound-induced lung hemorrhage is not caused by inertial cavitation' [J. Acoust. Soc. Am. **108**, 1290–1297 (2001)]," J. Acoust. Soc. Am. **110**, 1737 (2001).
[19] L. A. Frizzell, J. M. Kramer, J. F. Zachary, and W. D. O'Brien, Jr., "Response to "Comment on 'Ultrasound-induced lung hemorrhage is not caused by inertial cavitation'" [J. Acoust. Soc. Am. **110**, 1737 (2001)]," J. Acoust. Soc. Am. **110**, 1738–1739 (2001).
[20] R. E. Apfel, "Reply to Frizzell *et al.*'s comment to our comment," J. Acoust. Soc. Am. **110**, 1740–1741 (2001).
[21] L. A. Frizzell, J. M. Kramer, J. F. Zachary, and W. D. O'Brien, Jr., "Comment on Apfel's second comment," J. Acoust. Soc. Am. **110**, 1742 (2001).
[22] C. K. Holland, C. X. Deng, R. E. Apfel, J. L. Alderman, L. A. Fernandez, and K. J. Taylor, "Direct evidence of cavitation in vivo from diagnostic ultrasound," Ultrasound Med. Biol. **22**, 917–925 (1996).
[23] W. D. O'Brien, Jr., L. A. Frizzell, R. M. Weigel, and J. F. Zachary, "Ultrasound-induced lung hemorrhage is not caused by inertial cavitation," J. Acoust. Soc. Am. **108**, 1290–1297 (2000).
[24] M. L. Crosfill and J. G. Widdicombe, "Physical characteristics of the chest and lungs and the work of breathing in different mammalian species," J. Physiol. (London) **158**, 1–14 (1961).
[25] S. M. Tenney and J. E. Remmers, "Comparative quantitative morphology of the mammalian lung: Diffusing area," Nature (London) **197**, 54–56 (1963).
[26] E. R. Weibel, "Dimensions of the tracheobronchial tree and alveoli," in *Biological Handbooks: Respiration and Circulation*, edited by P. L. Altman and D. S. Dittmer (Federation of American Societies for Experimental Biology, Bethesda, MD, 1971), Chap. 51.
[27] W. D. O'Brien, Jr., J. M. Kramer, T. G. Waldrop, L. A. Frizzell, R. J. Miller, J. P. Blue, and J. F. Zachary, "Ultrasound-induced lung hemorrhage: Role of acoustic boundary conditions at the pleural surface," J. Acoust. Soc. Am. **111**, 1102–1109 (2002).
[28] T. J. Bauld and H. P. Schwan, "Attenuation and reflection of ultrasound in canine lung tissue," J. Acoust. Soc. Am. **56**, 1630–1637 (1974).
[29] F. Dunn and W. J. Fry, "Ultrasonic absorption and reflection by lung tissue," Phys. Med. Biol. **5**, 401–410 (1961).
[30] F. Dunn, "Attenuation and speed of ultrasound in lung," J. Acoust. Soc. Am. **56**, 1638–1639 (1974).
[31] F. Dunn, "Attenuation and speed of ultrasound in lung: Dependence upon frequency and inflation," J. Acoust. Soc. Am. **80**, 1248–1250 (1986).
[32] P. C. Pederson and H. S. Ozcan, "Ultrasound properties of lung tissue and

their measurements,'' Ultrasound Med. Biol. **12**, 483–499 (1986).
[33] Z. Mikhak and P. C. Pederson, ''Acoustic attenuation properties of the lung: An open question,'' Ultrasound Med. Biol. **28**, 1209–1216 (2002).
[34] L. E. Kinsler, A. R. Frey, A. B. Coppens, and J. V. Sanders, *Fundamentals of Acoustics*, 3rd ed. (Wiley, New York, 1982).
[35] F. Dunn, P. D. Edmonds, and W. J. Fry, ''Absorption and dispersion of ultrasound in biological media,'' in *Biological Engineering*, edited by H. P. Schwan (McGraw Hill, New York, 1969), pp. 205–332.
[36] H. Bachofen, A. Amman, D. Wangensteen, and E. R. Weibel, ''Perfusion fixation of lungs for structure-function analysis: Credits and limitations,'' J. Appl. Physiol.: Respir., Environ. Exercise Physiol. **53**(2), 528–533 (1982).
[37] G. Hayatdavoudi, J. D. Crapo, F. J. Miller, and J. J. O'Neil, ''Factors determining degree of inflation in intratracheally fixed rat lungs,'' J. Appl. Physiol.: Respir., Environ. Exercise Physiol. **48**(2), 389–393 (1980).
[38] J. Neter, M. H. Kutner, C. J. Nachtsheim, and W. Wasserman, *Applied Linear Statistical Models*, 4th ed. (Irwin, Chicago, 1996), Chaps. 1–2, pp. 3–94.